Energetic neutral atoms at Mars: 2. Imaging of the solar wind–Phobos interaction

ARTICLE *in* JOURNAL OF GEOPHYSICAL RESEARCH ATMOSPHERES · JANUARY 1278

Impact Factor: 3.43 · DOI: 10.1029/2001JA000328

Energetic neutral atoms at Mars
2. Imaging of the solar wind-Phobos interaction

Alessandro Mura, Anna Milillo, and Stefano Orsini
Istituto di Fisica dello Spazio Interplanetario, Consiglio Nazionale delle Ricerche, Rome, Italy

Esa Kallio
Finnish Meteorological Institute, Helsinki, Finland

Stas Barabash
Institutet för Rymdfysik, Kiruna, Sweden

Received 30 September 2001; revised 22 January 2002; accepted 23 January 2002; published 9 October 2002.

[1] The interactions between the solar wind and the neutral gas from Mars' moon Phobos and from the Martian exosphere are examined in order to check the feasibility of the energetic neutral atoms (ENA) remote sensing technique applied to Phobos' environment. Both solar wind and Mars exosphere models, as given in the literature, have been used. The density distribution of an outgassed neutral oxygen population located at Phobos' orbit has been simulated via Monte Carlo integration. Images and energy spectra of ENA, escaping through charge exchange processes, have been reconstructed applying a line of sight integration method. The performed simulation shows that the ENA signal originated from Phobos' environment is faint while observing far from Phobos location; anyway, it could be detected in some particular Mars-Phobos vantage point configurations. The possibility that the neutral oxygen outgassing rate might be estimated through ENA signal deconvolution is briefly discussed. *INDEX TERMS:* 6230 Planetology: Solar System Objects: Martian satellites; 6025 Planetology: Comets and Small Bodies: Interactions with solar wind plasma and fields; 5464 Planetology: Solid Surface Planets: Remote sensing; 5465 Planetology: Solid Surface Planets: Rings and dust; *KEYWORDS:* Phobos-Mars-solar wind interaction, satellite, ENA imaging, remote sensing

Citation: Mura, A., A. Milillo, S. Orsini, E. Kallio, and S. Barabash, Energetic neutral atoms at Mars, 2, Imaging of the solar wind-Phobos interaction, *J. Geophys. Res.*, *107*(A10), 1278, doi:10.1029/2001JA000328, 2002.

1. Introduction

[2] The purpose of this paper is to check the feasibility of imaging the Mars-Phobos ambient by detecting energetic neutral atoms, in the frame of the ASPERA-3 experiment on board of the ESA/Mars Express mission that will be launched in 2003. This instrument includes a neutral particle imager (NPI) with full 3D view and angular resolution of $10^\circ \times 5^\circ$, and a neutral particle detector (NPD) with $30^\circ \times 5^\circ$ angular resolution and 16 energy steps between 100 eV and 10 keV. During its mission, the Mars Express spacecraft will fly close to Phobos at distances down to 200 km for quite a few times. This opens up an exciting possibility to study the interactions of the Phobos' outgassing with the solar wind and prove (or disprove) the earlier finding made by ASPERA on board the PHOBOS-2 mission [*Dubinin et al.*, 1990]. More generally, ASPERA-3 will provide new opportunities for the study of the properties of solar wind protons [*Holmström et al.*, 2002], of the planetary energetic protons [*Lichtenegger et al.*, 2002], and of the planetary oxygen ions [*Barabash et al.*, 2002].

[3] The solar wind interacts with Mars and its natural satellites, mainly through direct impact with the ambient atmospheric/exospheric gas and the solid bodies of the satellites. Recent results of the MAG/GR instrument on board of Mars-Global-Surveyor showed that Mars has a nonhomogeneous and localized magnetic field of crustal origin [*Acuña et al.*, 1998, 1999, 2001]. Anyway, in a first approximation, the magnetic field effects on the global interaction between Mars and the solar wind may be assumed as marginal. Hence in the following we will consider Mars as a nonmagnetized planet.

[4] Given the previous assumptions, specific regions of interaction may be defined [e.g., *Vaisberg et al.*, 1990] as: (1) a bow shock, where the solar wind impacts the planetary environment; (2) a "magnetosheath," where the solar wind particles are deflected and mixed to planetary particles; (3) a "magnetopause," where the plasma speed decreases; (4) a "magnetosphere," where the energies slow down and the density increases; and (5) an obstacle boundary, no plasma or field penetrates it.

[5] Concerning Mars' natural satellites, Phobos and Deimos, we must take into account that a rocky body without a magnetic field and without an atmosphere interacts with the solar wind plasma only with its surface and with the outgassing material surrounding the body. Hence a bow

0148-0227/02/2001JA000328$09.00

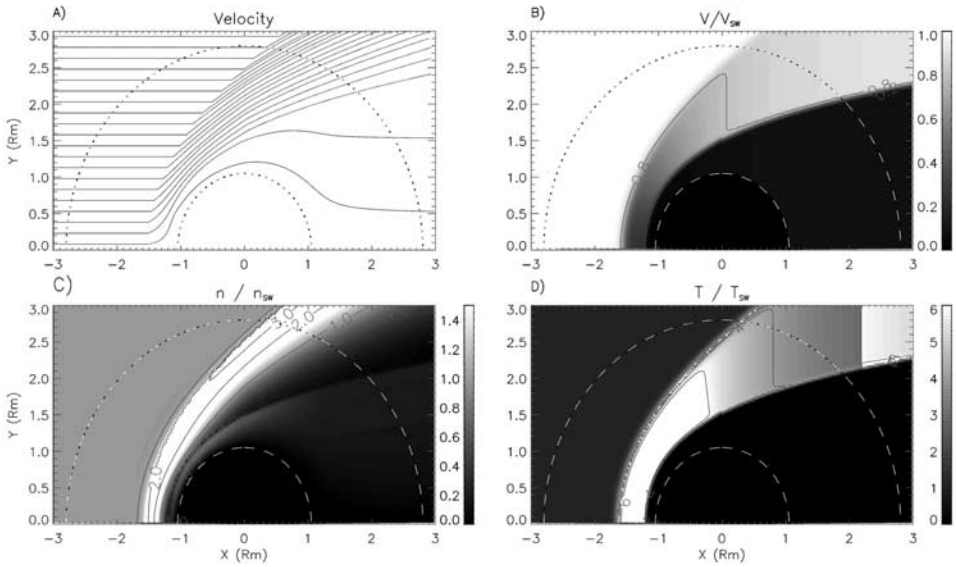

Figure 1. Empirical model of proton flux around Mars: (a) streamlines, (b) protons speed V/V_{SW}, (c) proton density n/n_{SW}, (d) proton temperature T/T_{SW} [from *Kallio*, 1996].

shock able to deflect the solar wind flow does not form around them.

[6] Here we investigate the solar wind interaction with the H, H_2 and O gas components of Mars/Phobos environment. When a H^+ collides with a neutral particle, it may charge exchange and be neutralized, becoming H^-ENA. The charge exchange is a symmetrical resonance process in the case of H target [*Hasted*, 1964], and an accidental resonance process in the cases of O target [*Stebbings et al.*, 1964] and H_2 target [*Hasted*, 1964]. Hence only a few eV are lost in this interaction, and the newly created ENA retains approximately both the energy of the colliding energetic ion and its direction (see section 5.3 for further details).

[7] If its mean free path is long enough, such ENA can transport information out of the generation region, thus allowing remote sensing of the interaction process [e.g., *Roelof et al.*, 1985; *Roelof*, 1987; *Henderson et al.*, 1997; *Orsini and Milillo*, 1999; *Milillo and Orsini*, 2001].

[8] Charge exchange processes are expected to be very effective at Mars, because the solar wind can reach altitudes where the density of the atmospheric neutrals is quite high (up to 10^6 cm^{-3}). Hence ENAs imaging is a potentially useful tool for understanding the geometry, the physics, and the dynamics of the plasma around Mars. [e.g., *Kallio et al.*, 1997].

[9] Mars closest satellite, Phobos, is orbiting nearby the equatorial plane of the planet at a distance of about 2.7 R_M from Mars. Outgassing phenomena may produce a gas torus along its orbit [e.g., *Ip and Banaszkiewicz*, 1990; *Horanyi et al.*, 1990; *Dubinin et al.*, 1990, 1991]. In this paper, we show that a denser neutral population should also be present closer to the satellite. Phobos' orbit is partially embedded in the Martian magnetosheath (in the dusk and dawn sectors) and in the magnetosphere (in the nightside). Hence its outgassing material may interact not only with the undisturbed solar wind, but also with the plasma flowing around Mars [e.g., *Barabash and Lundin*, 1994].

[10] The described interaction can produce a supplementary ENA signal near the satellite as well as along its orbit. This signal could be detected from appropriate vantage points, and discriminated from the background ENA signal of Martian origin. In this way, new information on Phobos environment could be achieved.

[11] In section 2, we discuss the model of plasma distribution in the Martian environment and the characteristics of Mars' atmosphere and exosphere, considered as a basic reference for our analyses. Then, we add the outgassing neutral population coming from Phobos, which generates a torus along its orbit as well as a halo around it. In section 3, we describe the ENA simulation method, and in section 4 we show the resulting simulated ENA images from both Mars and Phobos. In section 5, we discuss the shape of Phobos' torus with the intent to obtain an estimation of the outgassing rate by analyzing the ENA signal. In the end of this section, possible improvements of the described procedures are highlighted. Finally, in section 6 we summarize the main results.

2. Models Description

2.1. Proton Flux Model

[12] The empirical model of the proton flow is based on ASPERA three-dimensional proton velocity measurements, and is ascribed to *Kallio* [1996]. It gives proton velocity, density and temperature in a bidimensional plane, postulating an axial symmetry around Sun-Mars axis. A gas dynamic relationship is used to approximate the proton temperature in the magnetosheath and in the magnetosphere. The model includes a bow shock, a magnetopause and an inner obstacle boundary, which, here, is a sphere of radius equal to 1.05 Mars' radii (R_M). This model involves streamlines that penetrate the magnetopause in the wake as well as on the dayside [*Kallio et al.*, 1997]. The presence of Phobos does not modify the model. In fact, due to its very small dimensions, Phobos is not able to deflect the proton

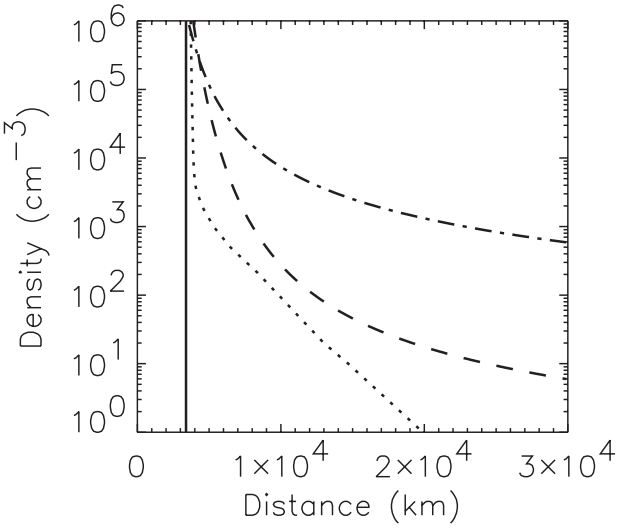

Figure 2. Neutral particle density profiles in the Martian exosphere versus altitude: oxygen (dotted), hydrogen (dash-dotted), and molecular hydrogen (dashed) [from *Krasnopolsky and Gladstone*, 1996]. The solid line indicates the Mars surface.

flux. Figure 1 shows maps of the streamlines, the velocity, the density, and the temperature of the proton flows around Mars, as modeled by *Kallio* [1996]. The inner circumference shows the position of the planetary obstacle boundary, while the outer one shows the position of Phobos orbit. It is worth to notice here that, according to this model, half of Phobos' orbit is inside the bow shock.

2.2. Models of Neutral Atom Distributions

2.2.1. Mars' Atmosphere and Exosphere

[13] Our simplified model considers Mars' atmosphere and exosphere as composed only of oxygen, hydrogen, and molecular hydrogen. It is known that helium is also present in Mars environment [*Krasnopolsky and Gladstone*, 1996], but its presence has not been taken into account, due to its lower charge exchange cross section. The neutral profiles for hydrogen populations are approximated by exponential functions, depending on the exospheric temperature and on the distance from Mars [*Krasnopolsky and Gladstone*, 1996]. The oxygen population is made of a thermal component at low altitude plus a nonthermal corona [*Zhang et al.*, 1993a]. Figure 2 shows the density of those species versus distance from Mars during low solar activity. Since the exospheric temperature depends on solar activity and solar wind conditions, the neutral particle density profiles versus altitude show similar variability. For the same reason also the relative abundances show significant variations: during high activity the main contribution is due to oxygen, while during more quiet periods the hydrogen is the main atmospheric component [*Kallio et al.*, 1997]. In this paper, we concentrate our analysis on the low-activity periods.

2.2.2. Phobos' Gas Torus and Halo

[14] Phobos is the natural satellite closest to the planet. Its orbit, located on the ecliptic plane, is approximately circular, at 9500 km from Mars (R_{MP}); the orbital period is 7 hours. It is an irregular object with an average radius of about 10 km; its mass is only 10^{-8} times the mass of Mars. It has been suggested that Phobos may contain water [e.g., *Fanale and Salvail*, 1989], and that surface-outgassing phenomena may occur. If the escaping velocity of an outgassing particle is small compared to that of Phobos, this particle is trapped in a keplerian orbit around Mars [*Ip and Banaszkiewicz*, 1990]. Hence all of the trapped particles fill a torus, which is, approximately, the envelope of all the permitted trajectories [*Krymskii et al*, 1992]. This torus is positioned on the ecliptic plane, and has an approximately circular cross section. Both the dimension of the torus and the related density of neutrals depend on the velocity distribution of the escaping particles, on the neutrals loss-decay time τ and on the surface outgassing rate $dN/dt = Q$, where N is the number of particles. *Sauer et al.* [1995], when attempting to model the Deimos interaction with solar wind, show that an outgassing rate of 10^{23} s^{-1} would be consistent with PHOBOS-2 IMF and plasma data. Moreover, *Krymskii et al.* [1992] and *Ip and Banaszkiewicz* [1990] show that such a rate could be considered as a basic reference also for Phobos outgassing. With an oxygen outgassing rate $Q = 10^{23}$ s^{-1}, for a lifetime $\tau = 2 \times 10^6$ s (see section 5.1), and for a total volume V of 10^{25} cm^3 [e.g., *Ip and Banaszkiewicz*, 1990; *Krymskii et al*, 1992], the average neutral oxygen density ($\langle n_o \rangle$) inside the torus is:

$$\langle n_o \rangle = \frac{N}{V} = \frac{Q\tau}{V}. \tag{1}$$

By using the given quantities, it follows that $\langle n_o \rangle \sim 10^4$ cm^{-3}.

[15] Close to Phobos, the gas density is higher. In fact, under the hypothesis of a free expansion from Phobos, the oxygen density near the satellite is:

$$n_o = \frac{dN}{dV} = \frac{dN}{4\pi r_P^2 dr_P} = \frac{1}{4\pi r_P^2}\frac{dN}{dt}\frac{dt}{dr_P} = \frac{Q}{4\pi r_P^2 v_n}; \tag{2}$$

where r_P is the distance from Phobos and $v_n = dr_P/dt$ is the mean escape velocity. If $T_P = 250$ K is the surface temperature of Phobos, and m_O is the oxygen mass, $v_n = (2kT_P/m_O)^{1/2} = 500$ m s^{-1} [*Ip and Banaszkiewicz*, 1990; *Krymskii et al*, 1992]. The resulting n_o may be up to 10^6 cm^{-3}.

[16] In order to better estimate the density function inside this torus, we have simulated the trajectories of 10^7 test particles, escaping from Phobos with initial velocity randomly distributed. The lifetime of each test particle has been set equal to τ. At any chosen time t_0, each particle i, actually contributing to the total gas density, may be considered as outgassed at instant $t_0 - T_i$, where T_i is chosen randomly between 0 and τ. Then, each trajectory has been integrated in Phobos noninertial frame, with steps of 0.1 s, from $t_0 - T_i$ to t_0, taking into account Mars gravity, as well as centrifugal and Coriolis force. The gravity of Phobos has not been considered here because, in any point of space, it is less than 1% of that of Mars.

[17] In the model, each test particle starts moving from Phobos along a random direction, and the magnitude of the initial velocity is randomly distributed around its mean value v_n following Maxwell's law. Due to its small dimensions, Phobos may be considered as a point located in the origin of the reference frame. Hence each test particle starts

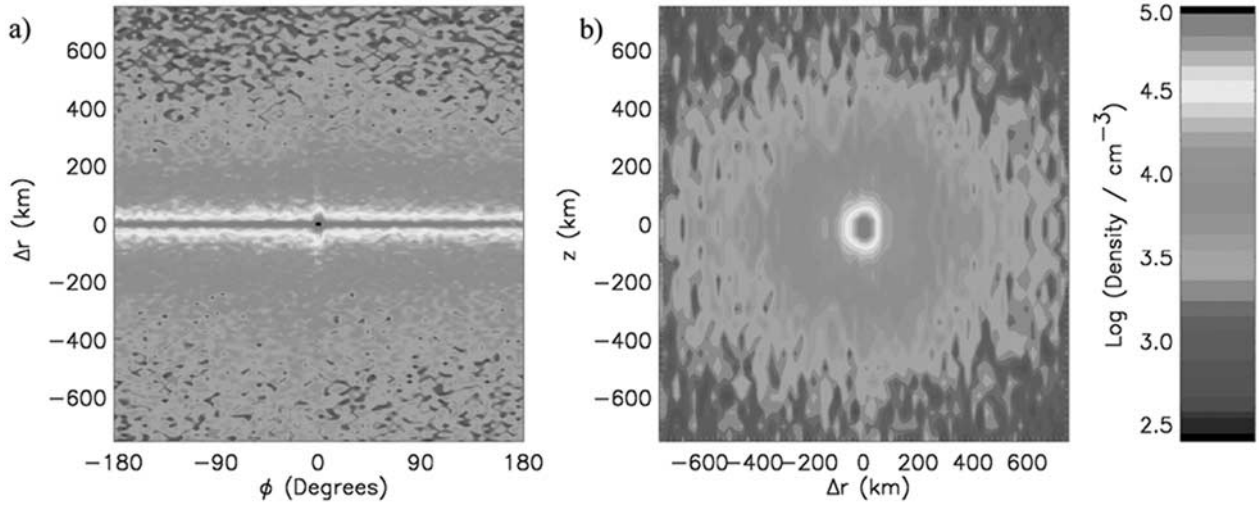

Figure 3. Simulated neutral oxygen density near the orbit of Phobos for different bidimensional sections: (a) ϕ versus r, $z = 0$; (b) Δr versus z, $\phi = 0$; $Q = 10^{23}$ s^{-1}. Phobos' position is at $\Delta r = 0$, $\phi = 0°$, $z = 0$; its velocity is directed toward the increasing ϕ. See color version of this figure at back of this issue.

its motion in the origin, and any subsequent impact between the particle and Phobos is neglected.

[18] Since the integration time T_i of a test particle is often greater than its orbital period around Mars, it is not necessary to numerically integrate the trajectory of a particle over the entire time T_i. In fact, each test particle moves around Mars an integer number of times m_i, plus an extra time ΔT_i equal to:

$$\Delta T_i = T_i - m_i T_i^*, \tag{3}$$

where T_i^* is the period of a full orbit around Mars in its inertial frame. According to Kepler's law, the orbital period can be written:

$$T_i^* = T_P \left(\frac{\eta_i}{R_{MP}} \right)^{3/2}, \tag{4}$$

and where η_i is the main axes of the i-particle elliptical orbit around Mars, in its inertial frame, and T_P is Phobos orbital period. Since we do know the total energy and the momentum at starting time t_0, it is easy to find using energy and momentum conservation laws [e.g., *Hodges*, 1994].

[19] Hence at instant $t_0 - \Delta T_i$, the test particle is in the same position as at instant $t_0 - T_i$, in Mars' inertial frame. It is easy to calculate the position of the particle at instant $t_0 - \Delta T_i$ in Phobos' noninertial frame, and then integrate the motion via numerical computation only on the residual time ΔT_i. The precession of the i-particle orbit due to Mars motion around the Sun has been neglected. The space around Mars has been divided into cells, based on a three-dimensional grid in cylindrical coordinates centered on Mars:

- r, the distance from Mars, with a 20 km resolution;
- z, the altitude above the ecliptic plane, with a 20 km resolution;
- ϕ, the angle between the particle and Phobos, with a resolution of 15°.

[20] The gas density n_{ijk} inside the generic cell of volume V_{ijk} has been assumed proportional to (number of particles)/V_{ijk} at instant t_0. Finally, the density has been normalized in order to have:

$$\sum_i \sum_j \sum_k n_{ijk} V_{ijk} = \tau Q. \tag{5}$$

The two panels of Figure 3 show the derived gas density distribution on two distinct bidimensional sections: ϕ, $r = r - R_{mp}$, $z = 0$. (Panel A), and z, Δr, $\phi = 0$. (Panel B). The halo density profiles, located in a small quasi-circular region surrounding Phobos, reach values up to 2×10^5 cm^{-3}. The torus along the orbit of Phobos exhibits density versus r profiles almost ϕ-independent, with a peak of $\approx 3 \times 10^4$ cm^{-3}.

3. Method for ENA Simulation Through Line of Sight Integration

[21] The differential ENA flux observed, for any energy and line of sight, at a given vantage point S_0, is generated by the interaction of the energetic ion fluxes with the ambient neutral gas. Concerning ion fluxes, only protons, characterized by a Maxwellian velocity distribution function, are considered in the present study. At each point S along the line of sight, the velocity distribution function $f(l, \mathbf{v})$ is:

$$f(l, \mathbf{v}) = \left(\frac{1}{\pi w(l)^2} \right)^{3/2} e^{\left(-\frac{|(\mathbf{v} - \mathbf{u}(l))|^2}{w(l)^2} \right)}; \tag{6}$$

where l is the distance $S - S_0$, u(l) is the mean proton velocity and w is the thermal velocity defined as:

$$w(l) = \left(\frac{2kT(l)}{m_{H^+}} \right)^{1/2}. \tag{7}$$

[22] Here, T is the solar wind temperature as in the proton flux model shown in section 2.1, k is the Boltzmann constant, and m_{H^+} is the proton mass. So at point S the proton infinitesimal flux dJ_{H^+}, directed toward S_0, is:

$$dJ_{H^+} = n_{H^+}(l) v f(l, \mathbf{v}) d\mathbf{v}, \tag{8}$$

where $n_{H+}(l)$ is the proton density.

[23] By expressing $f(l,\mathbf{v})$ as a function of l, kinetic energy E and direction $\hat{v}$

$$f'(l, E, \hat{v}) dE d\Omega = f(l, \mathbf{v}) d\mathbf{v} \tag{9}$$

where $d\Omega$ is the infinitesimal solid angle, we may estimate the ENA infinitesimal flux $dJ_{ENA}(E, \hat{v})$ and the ENA differential flux integrated along a certain line of sight $\Phi_{ENA}(E, \hat{v})$ as:

$$\begin{aligned} dJ_{ENA}(E,\hat{v}) &= \int_{l=0}^{l=\infty} dJ_{H^+} \sum_k \sigma_k n_k(l) \\ dr &= \int_{l=0}^{l=\infty} \left(\frac{2E}{m_{H^+}}\right)^{1/2} f'(l, E, \hat{v}) \sum_k \sigma_k n_k(l) n_{H^+}(l) dl \; dE \; d\Omega \\ \Phi_{ENA}(E,\hat{v}) &= \frac{dJ_{ENA}(E,\hat{v})}{dE \; d\Omega} \\ &= \int_{l=0}^{l=\infty} \left(\frac{2E}{m_{H^+}}\right)^{1/2} f'(l, E, \hat{v}) \sum_k \sigma_k n_k(l) n_{H^+}(l) dl, \end{aligned} \tag{10}$$

where n_k is the density of any neutral species, σ_k is the charge exchange cross section between protons and the k^{th} neutral species (H, H_2, O), as shown in Figure 4.

4. Hydrogen ENA Images and Spectra Simulation

[24] The hydrogen ENA flux examined here results from charge exchange processes occurring between the solar wind protons and the thermal neutral gas. This flux originates from two different regions: Mars' exosphere and Phobos' halo. However, due to the small dimensions of the Phobos' halo (see Figure 3), only at particular vantage points the related ENA signal (mixed with the stronger signal originating from Mars' exosphere) is sufficiently high to be discriminated. More particularly, the best configuration for detecting such a signal requires a vantage point located on Mars' equatorial plane.

[25] An example of Mars' exospheric ENA image, considered here as the background signal, is shown in Figure 5a. The Mars-Solar-Ecliptic (MSE) coordinates of the chosen vantage point S_0 are $x_{So} = -1.3\ R_M$, $y_{So} = 2.9\ R_M$, $z_{So} = 0\ R_M$, where R_M is Mars' radius (see Figure 5d). The dotted line represents Mars' obstacle boundary. In this case, the numerical integration of equation (10) has been performed with $dl = 0.01\ R_M$. The ENA differential flux with angular resolution $\Delta\theta = 2^\circ$ is integrated over all energies, from 1 eV to 2 keV. The figure shows clearly two different peaks: a narrow one centered on the sunward direction, and a more extended one close to the planet. The first is due to the ENA flux generated directly by the interaction between the solar wind outside the bow shock and the outer exosphere. The second is related to the signal resulting from the interaction between the thermalized solar wind inside the magnetosheath and the inner exosphere. The simultaneous observation of these two separate ENA regions clearly indicates that the vantage point is downstream of the Martian bow shock. It is worth to notice that the obtained ENA fluxes are in good agreement with those calculated by *Kallio et al.* [1997], who used an alternative approach based on a Monte Carlo method.

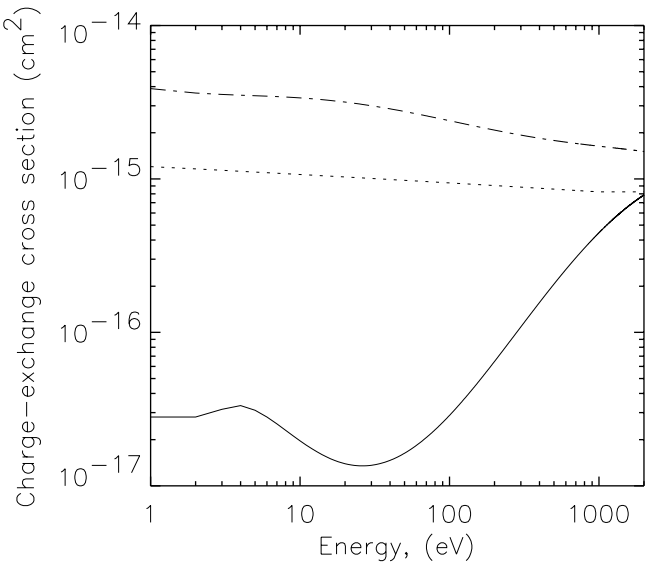

Figure 4. Cross section for charge exchange process between protons and hydrogen (dash-dotted) [*Barnett*, 1990], oxygen (dotted) [*Stebbings et al.*, 1964], and molecular hydrogen (solid) [*Barnett*, 1990] versus energy.

[26] Figure 5b shows the ENA signal generated by Phobos' neutral population (with the exclusion of the background signal reported in Figure 5a), assuming hypothetically that $Q = 10^{23}\ s^{-1}$ (see previous comments in section 2.2.2). The vantage point is the same as in Figure 5a; Phobos' MSE coordinates are: $x_P = -0.9\ R_M$, $y_P = 2.6\ R_M$, $z_P = 0\ R_M$ (see Figure 5d).

[27] The overall ENA image (Figure 5c) would result from the superposition of the two simulated pictures shown in Figures 5a and 5b. For almost all directions, the background from Mars' environment obscures the signal from Phobos. Nonetheless, the Phobos' ENA flux in between 40^0–60^0 on Mars' equatorial plane is higher and detectable.

[28] Figure 6 shows the ENA spectra relative to Figure 5, integrated over all directions in the sky. The spectrum related to Mars' ENA flux (solid line) is the envelope of the fluxes from three different regions. The signal at lower energy (2–6 eV) is generated close to Mars surface, where the energy of the proton flux is low (subsolar point). The signal at higher energy (0.4–2 keV) results from interaction of neutral gas with unperturbed solar wind outside the bow shock (~1–2 keV), as well as deflected solar wind in the magnetosheath.

[29] Phobos' ENA energy spectrum (dashed line) exhibits a trend similar to the previous one. On the other hand, its

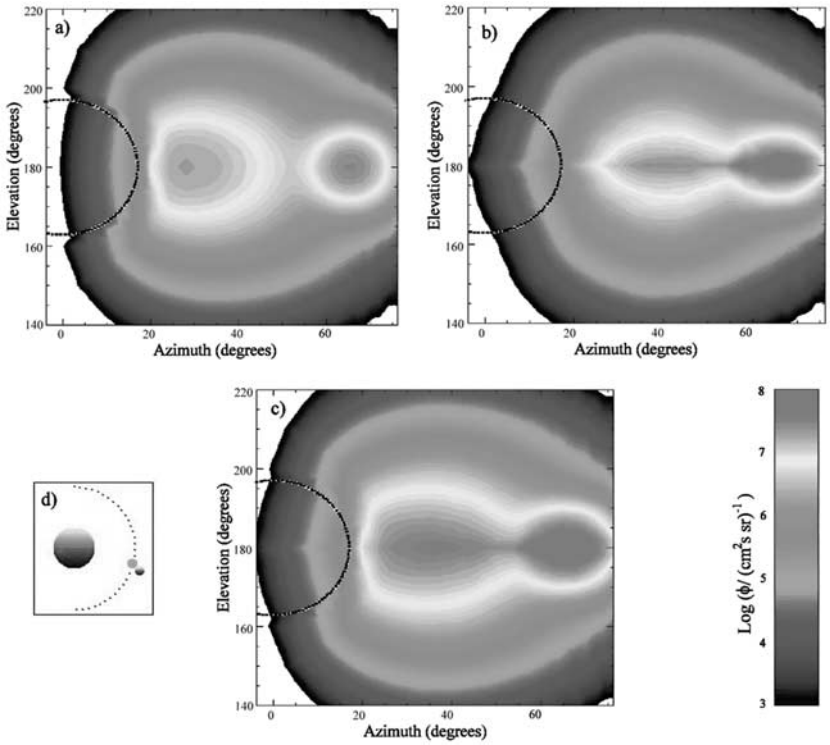

Figure 5. (a) Pseudocolor map of the ENA differential flux, function of the elevation and azimuth angle, if only Mars exosphere was present. The dashed line represents Mars' obstacle boundary. Azimuth angle is measured on the equatorial plane, beginning from Mars' center; elevation angle is measured perpendicular to the equatorial plane, Mars' center is at 180°. (b) Same as Figure 5a, if only Phobos torus-halo was present. (c) Overall ENA image resulting from the superposition of Figures 5a and 5b. The flux is integrated over all energy from 1 eV to 2 keV. (d) The spheres show an equatorial view of the relative positions of Mars (red), Phobos (blue), and the vantage point (gray); the Sun is up. See color version of this figure at back of this issue.

intensity is comparable to Mars' ENA spectrum only in the 0.4–2 keV range. This is due to the position of Phobos' orbit, which allows the halo-torus neutral gas to interact only with the unperturbed or magnetosheath solar wind.

5. Discussion

[30] In our study, we have analyzed the characteristics of the oxygen neutral population, outgassed from Phobos, and distributed along its orbit around Mars. Furthermore, we have attempted to interpret the ENA signal originated through charge exchange between such a neutral gas and the directional proton flux.

5.1. Phobos' Neutral Oxygen Distribution

[31] Phobos' neutral oxygen distribution function has been reconstructed via Monte Carlo simulation. Usually, this approach allows getting information about the density distribution from the entire test particle trajectory [e.g., *Hodges*, 1994], which could be obtained by using numerical or analytical computations. However, in our case this simple method is subjected to two significant limitations: (1) the trajectory of a test atom is too long to allow numerical integration of the motion without large computational errors; (2) the presence of noninertial forces makes the analytical approach difficult to perform. In the case of long

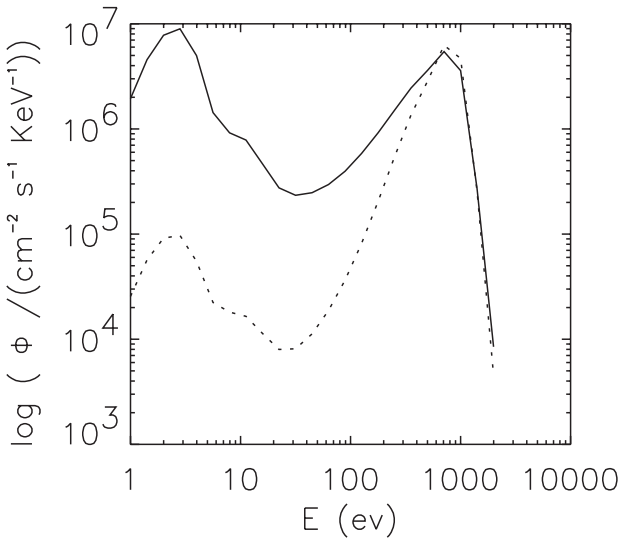

Figure 6. Spectra of the ENA fluxes coming from Mars (solid line) and Phobos (dotted line), integrated over all directions in the sky. Vantage point and Phobos position are the same as in Figure 5.

trajectories in noninertial frames, the only way to solve this problem is to use first analytical and then numerical computations (see section 2.2.2).

[32] It is possible to find an analytical function, which fits the empirical data. With the exclusion of Phobos' halo, the neutral density on the $z = 0$ plane can be estimated by a very simple function with only two free parameters:

$$n(r, \phi) = \frac{A}{B + \mid r - R_{MP} \mid}, \tag{11}$$

where $A = 7.25 \times 10^8 \pm 7.17 \times 10^6$, and $B = 1.20 \times 10^4 \pm 2.30 \times 10^2$, if n is expressed in cm^{-3} and r is expressed in m. The correlation coefficient between this function and the data is 0.996. This function may be easily extended to the whole space around Phobos' orbit, since the cross section of the torus is approximately circular (see Figure 3b).

[33] The discussed distribution is obviously influenced by loss processes. There are three main causes of O atom ionization in Phobos' torus: charge exchange, photoionization and electron impact ionization. All of the mentioned processes do produce significant loss of neutral gas. In fact, after ionization, oxygen is supposed to be removed by Jeans escape and solar wind capture. The detailed estimate of the relative contribution of the mentioned processes would need a careful analysis of the plasma circulation around Phobos. A zero-order estimate could be based on solar wind plasma features, taking into account that Phobos is embedded by solar wind-like plasma for more than half of its period. With this assumption, the proton velocity $V_{SW} = 4 \times 10^7$ cm s^{-1}, and density $n_{SW} = 2.5$ cm^{-3} may be considered. This yields a proton flux of 1×10^8 cm^{-2} s^{-1}. Taking into account the H^+-O charge exchange cross section (see Figure 4), we obtain a charge exchange frequency $f_{CE} = 10^{-7}$ s^{-1}. It is worth noticing that charge exchange effect is comparable to other loss processes. As a matter of fact, at Mars' orbit, during solar minimum, the photoionization frequency is $f_\gamma = 10^{-7}$ s^{-1}, and the electron impact ionization frequency is $f_e = 2 \times 10^{-7}$ s^{-1} [*Zhang et al.*, 1993b]. The total loss frequency f is then the sum of all these frequencies ($f = 4 \times 10^{-7}$ s^{-1}). Hence we have generally considered an oxygen gas lifetime $\tau = f^{-1} = 2 \times 10^6$ s (see section 2.2.2).

5.2. ENA Signal Analysis and Outgassing Rate Estimation

[34] From these simulations, it results that the ENA flux generated close to Phobos is detectable, but only for particular configurations. As an example, in Figure 5 we have analyzed the ENA signal if detected from a vantage point located on Mars' equator. The chosen $80° \times 80°$ field of view is centered on a line of sight parallel to the deflected solar wind direction. The Sun direction is inside the field of view; the Sun is a source of strong background noise, due to both the photon radiation and the unperturbed solar wind ENA signal. Nevertheless, from Figure 5 it appears that most of the incoming signal from Phobos can be discriminated from this background. The signal is, of course, maximum in the equatorial plane. We have simulated ENA images and spectra for many different Mars-Phobos vantage point configurations, and observed that if the vantage point is placed outside from the equatorial plane, the ENA flux from Phobos becomes very weak, and hardly detectable.

[35] The neutral density from Phobos depends on the outgassing rate Q as well as on the mean lifetime τ. The shape of the distribution, however, depends only on τ, which is known with a sufficient accuracy [*Zhang et al.*, 1993b]. Hence the neutral density originated from Phobos, as well as the related ENA signal, are simply proportional to Q (see equations (5) and (9)). From our simulation, it results that the presence of a neutral population originated from Phobos induces an extra ENA signal that is detectable. This potentially allows the estimate of Q by analyzing the ENA signal.

5.3. Model Limits and Future Improvements

[36] In the present study a preliminary analysis of the interaction between the solar wind and the Mars/Phobos system is performed. The properties of the system environment, as well as those of the nearby solar wind are not well known. Therefore the used analytical model of the ion flux includes several free parameters to control the properties of the plasma near the planet, like the height of the obstacle boundary, the magnetopause location and shape, and others. Moreover, we are forced to make some assumptions on the neutral distribution of the system. Further improvements to the present analysis could be better modeling of: (1) the proton flux (including the nonhomogeneous and localized magnetic field effects [*Acuña et al.*, 2001]), (2) the exospheric neutral density (presently approximated by an exponential extrapolation that overstates densities at great distances), (3) the fast-oxygen corona (up to altitudes 7000 km form the surface [e.g., *Hodges*, 2000; *Kim et al.*, 1998])

[37] In the present study, the solar activity is assumed low. However, solar activity fluctuations should be considered, since the exospheric temperature depends on solar activity and solar wind conditions, the neutral particle density profiles versus altitude show similar variability. For the same reason also the relative abundances show significant variations: during high activity the main contribution is due to oxygen, while during more quiet periods the hydrogen is the main atmospheric component [*Kallio et al.*, 1997]. Hence the resulting ENA fluxes could be different during high activities.

[38] Energetic O^+ ions (not considered here) of planetary origin have been detected both in the flanks of the Martian magnetosphere and in the central tail by Phobos/ASPERA instrument [*Kallio et al.*, 1995]. The charge exchange between the neutrals and the oxygen ions could be effective in the Mars environment [*Kallio and Koskinen*, 1998].

[39] The simplified outgassed neutral population considers oxygen as the only constituent. This simplification comes out from the fact that such a population has been effectively hypothesized by *Dubinin et al.* [1990]. A more sophisticated model should eventually include all of the possible components/phenomena.

[40] The ENA imaging technique is based on the assumption that, after charge exchange process, the H-ENA retains the energy and the direction of the incoming proton. In the

case of an asymmetric/accidental resonance process (like H^+-O), the energy variation (a few eV) may be assumed as negligible in our case [*Stebbings et al.*, 1964]. The differential cross section $\frac{d\sigma(\theta)}{d\Omega}$, in the energy range between 500 eV and 5 keV, strongly peaks in the forward direction (within 2.5°), even if large scattering angles may occur [*Lindslay et al.*, 1996]. The presence of a scattering angle in the charge exchange process may result in a blurring of the ENA images. In the present study, such an effect has not been taken into account. In fact, the H-ENA flux originated from H^+-O interaction comes from both Mars' and Phobos' environments. However, the bulk of the H-ENA flux from Mars' environment is originated from H^+-H interactions (exhibiting a very low scattering), due to both the higher hydrogen density and the higher charge exchange cross section (see Figures 2 and 4). Hence the blurring of the total signal due to scattering may be neglected on first approximation. The H-ENA flux from Phobos is supposed to originate only from H^+-O interactions; the peak energy (see Figure 6) falls within the 0.5–5 keV range mentioned before. Generally, the related scattering should not be negligible even if, due to the small distance between the source and the vantage point, it should not strongly affect our results. Further improvements to the present analysis could consider the scattering angle of the charge exchange process, simply by increasing the temperature of the proton fluxes. In fact, we could simulate scattering at charge exchange process by adding to the proton temperature w (a free parameter of our model) a further free parameter Δw, due to scattering.

6. Conclusions

[41] One of the main aspects about Phobos' exosphere composition and outgassing rate is related to the presence of water on this Martian satellite; a definite clarification of such an intriguing issue would be of fundamental interest for determining the time evolution of Phobos [e.g., *Fanale and Salvail*, 1989]. In the present study, we have presented a method able to investigate Phobos' exosphere properties, by simulating the ENA signal generated through interaction between the solar wind and the outgassed neutrals. The simulations show that oxygen outgassing generates an ENA flux, whose signal may be discriminated from the background for particular positions of the vantage point. This technique can provide relevant information, useful for determining the major characteristics of neutral outgassing, whose rate has not been directly measured. This procedure may be improved by considering more neutral species, various solar activity conditions, and by adding a model for the local magnetic field.

[42] The simulated ENA signal will be tested with in situ measures: the ASPERA 3 instrument, on board the next ESA mission Mars Express that will be launched in 2003, will give the scientific community an opportunity to analyze the ENA signal from the Mars/Phobos system, hence procuring an important tool for the future of planetary investigation.

[43] **Acknowledgments.** Janet G. Luhmann thanks the referees for their assistance in evaluating this paper.

References

Acuña, M. H., et al., Magnetic field and plasma observations at Mars: Initial results of the Mars global surveyor mission, *Science*, *279*(5357), 1676, 1998.

Acuña, M. H., et al., Global distribution of crustal magnetism discovered by the Mars global surveyor MAG/ER experiment, *Science*, *284*(5415), 790, 1999.

Acuña, M. H., et al., Magnetic field of Mars: Summary of results from the aerobraking and mapping orbits, *J. Geophys. Res.*, *106*, 23,403, 2001.

Barabash, S., and R. Lundin, On a possible dust-plasma interaction at Mars, *IEEE Trans. Plasma Sci.*, *22*(2), 173, 1994.

Barabash, S., M. Holmström, A. Lukyanov, and E. Kallio, Energetic neutral atoms at Mars, 4, Imaging of the oxygen escape, *J. Geophys. Res.*, *107*, 10.1029/2001JA000326, in press, 2002.

Barnett, C. F., Collisions of H, H_2, He and Li atoms and ions with atoms and molecules, in *Atomic Data for Fusion Ser.*, vol. 1, *Rep. ORNL-6086*, edited by H. T. Hunter et al., Oak Ridge Nat. Lab., Oak Ridge, Tenn., 1990.

Dubinin, E. M., R. Lundin, N. F. Pissarenko, S. V. Barabash, A. Z. Zakharov, H. Koskinen, K. Schwingenschuh, and Y. G. Yeroshenko, Indirect evidences for a gas/dust torus along the Phobos orbit, *Geophys. Res. Lett.*, *17*, 861, 1990.

Dubinin, E. M., N. F. Pissarenko, S. V. Barabash, A. Z. Zakharov, R. Lundin, H. Koskinen, K. Schwingenschuh, and Y. G. Yeroshenko, Tails of Phobos and Deimos in the solar wind and in the Martian magnetosphere, *Planet. Space Sci.*, *39*(1), 123, 1991.

Fanale, F. P., and J. R. Salvail, Loss of water from Phobos, *Geophys. Res. Lett.*, *16*, 287, 1989.

Hasted, G. B., *Physics of Atomic Collisions*, 416 pp., Butterworths, London, 1964.

Henderson, M. G., G. D. Reeves, H. E. Spence, R. B. Sheldon, A. M. Jorgensen, J. B. Blake, and J. F. Fennell, First energetic neutral atom images from polar, *Geophys. Res. Lett.*, *24*, 1167, 1997.

Hodges, R. R., Jr., Monte Carlo simulation of terrestrial hydrogen exosphere, *J. Geophys. Res.*, *99*, 23,229, 1994.

Hodges, R. R., Jr., Distribution of hot oxygen for Venus and Mars, *J. Geophys. Res.*, *105*, 6971, 2000.

Holmström, M., S. Barabash, and E. Kallio, Energetic neutral atoms at Mars, 1, Imaging of solar wind protons, *J. Geophys. Res.*, *107*, 10.1029/2001JA000325, in press, 2002.

Horanyi, M., M. Tatrallyay, and J. G. Luhmann, Simulations of dust particles in the Martian environment, *Geophys. Res. Lett.*, *17*, 857, 1990.

Ip, W.-H., and M. Banaszkiewicz, On the dust/gas tori of Phobos and Deimos, *Geophys. Res. Lett.*, *17*, 857, 1990.

Kallio, E., An empirical model of the solar wind flow around Mars, *J. Geophys. Res.*, *101*, 11,133, 1996.

Kallio, E., and H. Koskinen, Ion acceleration in the Martian plasma environment, *Adv. Space Res.*, *21*, 573, 1998.

Kallio, E., H. Koskinen, S. Barabash, C. M. C. Nairn, and K. Schwingenschuh, Oxygen outflow in the Martian magnetotail, *Geophys. Res. Lett.*, *22*, 2449, 1995.

Kallio, E., J. G. Luhmann, and S. Barabash, Charge exchange near Mars: The solar wind absorption and energetic neutral atom production, *J. Geophys. Res.*, *102*, 22,183, 1997.

Kim, J., A. F. Nagy, J. L. Fox, and T. E. Cravens, Solar cycle variability of hot oxygen atoms at Mars, *J. Geophys. Res.*, *103*, 29,339, 1998.

Krasnopolsky, V. A., and G. R. Gladstone, Helium on Mars: EUVE and PHOBOS data and implications for Mars' evolution, *J. Geophys. Res.*, *101*, 11,765, 1996.

Krymskii, A. M., T. K. Breus, M. K. Dougherty, D. J. Southwood, and W. I. Axford, The electromagnetic effects of the solar wind interaction with the Phobos neutral gas halo and dust torus, *Planet. Space Sci.*, *40*(8), 1033, 1992.

Lichtenegger, H., H. Lammer, and W. Stumptner, Energetic neutral atoms at Mars, 3, Flux and energy distribution of planetary energetic H atoms, *J. Geophys. Res.*, *107*, 10.1029/2001JA000322, in press, 2002.

Lindslay, B. G., D. R. Sieglaff, D. A. Schafer, C. L. Hakes, K. A. Smith, and R. F. Stebbings, Charge transfer of 0.5-, 1.5-, and 5-keV protons with atomic oxygen: Absolute differential and integral cross sections, *Phys. Rev. A*, *53*, 212, 1996.

Milillo, A., and S. Orsini, Energetic neutral atoms: Potential merits and first observations, *Recent Res. Devel. Geophys. Res.*, *3*, 153, 2001.

Orsini, S., and A. Milillo, Magnetospheric plasma loss processes and energetic neutral atoms, *Nuovo Cimento C*, *22*(5), 633, 1999.

Roelof, E. C., Energetic neutral atom image of a storm-time ring current, *Geophys. Res. Lett.*, *14*, 652, 1987.

Roelof, E. C., D. G. Mitchell, and D. J. Williams, Energetic neutral atoms E 50 keV from the ring current: IMP 7/8 and ISEE 1, *J. Geophys. Res.*, *90*, 10,991, 1985.

Sauer, K., E. Dubinin, K. Baumgartel, and A. Bogdanov, Deimos: An obstacle to the solar wind, *Science*, *269*, 1075, 1995.

Stebbings, R. F., C. H. Smith, and H. Ehrahardt, Charge transfer between oxygen atoms and O^+ and H^+ ions, *J. Geophys. Res.*, *69*, 2349, 1964.

Vaisberg, O. L., J. G. Luhmann, and C. T. Russell, Plasma observations of the solar wind interaction with Mars, *J. Geophys. Res.*, *95*, 14,841, 1990.

Zhang, M. H. G., J. G. Luhmann, S. W. Bougher, and A. F. Nagy, The ancient oxygen exosphere of Mars: Implication for atmosphere evolution, *J. Geophys. Res.*, *98*, 10,915, 1993a.

Zhang, M. H. G., J. G. Luhmann, A. F. Nagy, J. R. Spreiter, and S. S. Stahara, Oxygen ionization rates at Mars and Venus: Relative contribution of impact ionization and charge exchange, *J. Geophys. Res.*, *98*, 3311, 1993b.

S. Barabash, Swedish Institute of Space Physics, P.O. Box 812, SE-98128 Kiruna, Sweden. (stas@irf.se)

E. Kallio, Finnish Meteorological Institute, Vuorikatu 15 A, P.O. Box 503, FIN-00101 Helsinki, Finland. (Esa.Kallio@fmi.fi)

A. Milillo, A. Mura, and S. Orsini, Istituto di Fisica dello Spazio Interplanetario, CNR, via del Fosso del Cavaliere 100, I-00133 Roma, Italia. (anna.milillo@ifsi.rm.cnr.it; mura@ifsi.rm.cnr.it; stefano.orsini@ifsi.rm.cnr.it)

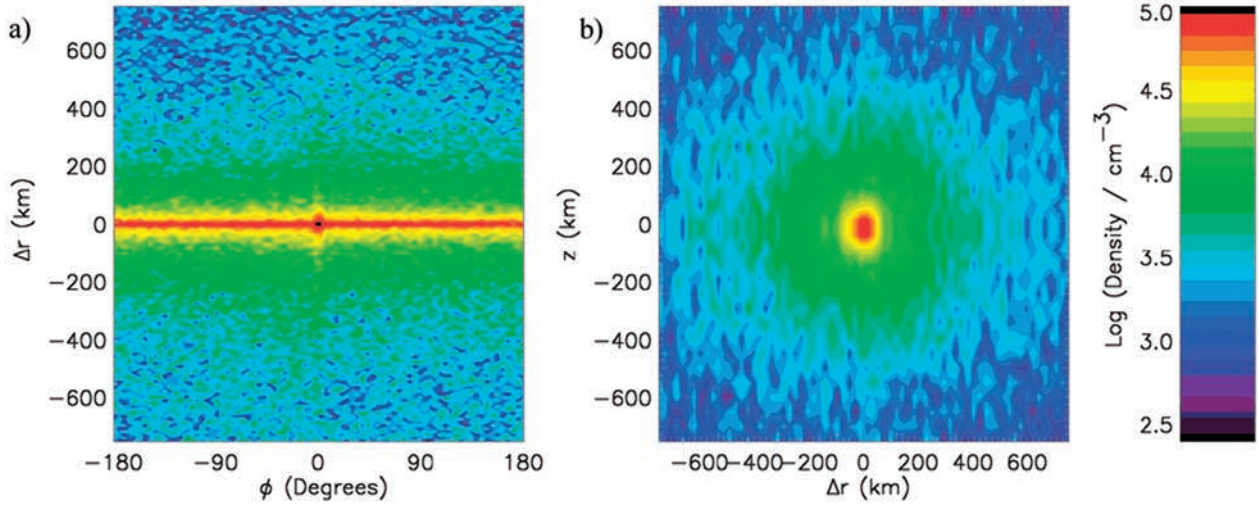

Figure 3. Simulated neutral oxygen density near the orbit of Phobos for different bidimensional sections: (a) ϕ versus r, $z = 0$; (b) Δr versus z, $\phi = 0$; $Q = 10^{23}$ s^{-1}. Phobos' position is at $\Delta r = 0$, $\phi = 0°$, $z = 0$; its velocity is directed toward the increasing ϕ.

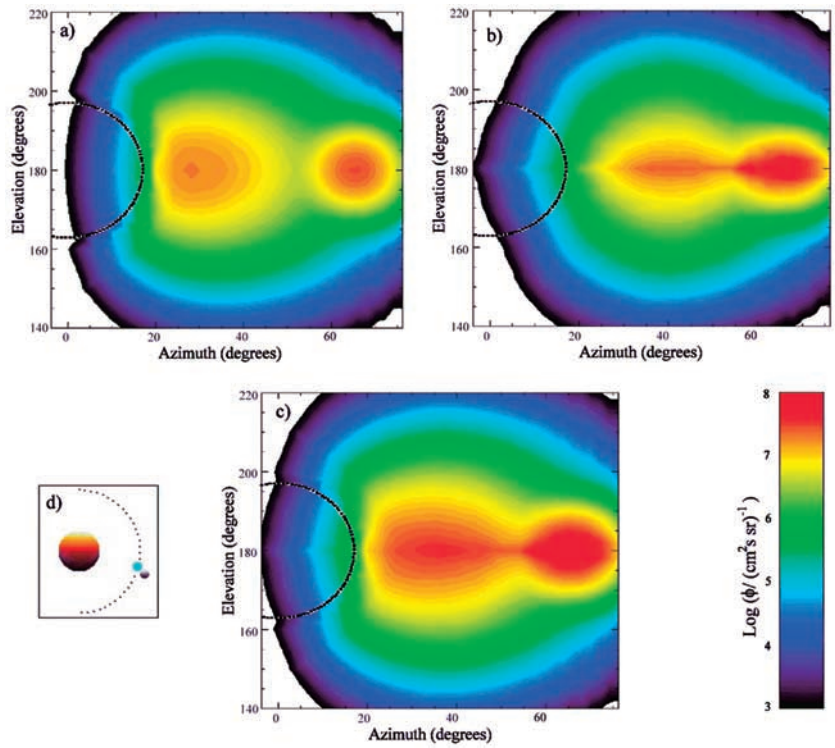

Figure 5. (a) Pseudocolor map of the ENA differential flux, function of the elevation and azimuth angle, if only Mars exosphere was present. The dashed line represents Mars' obstacle boundary. Azimuth angle is measured on the equatorial plane, beginning from Mars' center; elevation angle is measured perpendicular to the equatorial plane, Mars' center is at 180°. (b) Same as Figure 5a, if only Phobos torus-halo was present. (c) Overall ENA image resulting from the superposition of Figures 5a and 5b. The flux is integrated over all energy from 1 eV to 2 keV. (d) The spheres show an equatorial view of the relative positions of Mars (red), Phobos (blue), and the vantage point (gray); the Sun is up.